AD-A072 988 NAVAL RESEARCH LAB WASHINGTON DC F/G 21/2
FLAME - A SLOW-FLOW COMBUSTION MODEL,(U)
JUL 79 W W JONES, J P BORIS
UNCLASSIFIED NRL-MR-3970 NL

| OF |
ADA
072988

END
DATE
FILMED
9-79
DDC

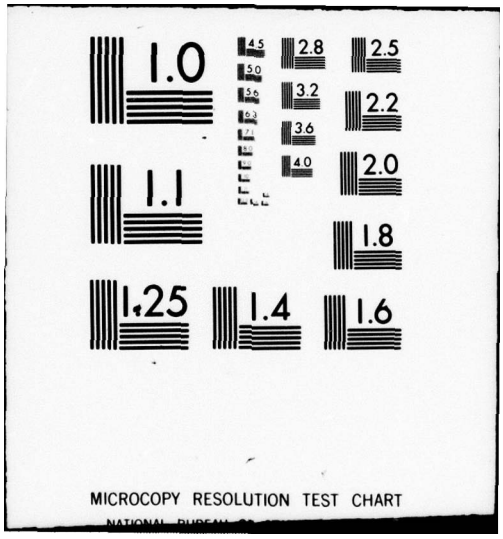
1.0
1.1
1.25
1.4
1.6
1.8
2.0
2.2
2.5
2.8
3.2
3.6
4.0
4.5
5.0
5.6
6.3
7.1
8.0
9.0
MICROCOPY RESOLUTION TEST CHART

NRL Memorandum Report 3970

Flame — A Slow-Flow Combustion Model

WALTER W. JONES AND J. P. BORIS

Laboratory for Computational Physics

July 16, 1979

NAVAL RESEARCH LABORATORY
Washington, D.C.

SECURITY CLASSIFICATION OF THIS PAGE (When Data Entered)

REPORT DOCUMENTATION PAGE

READ INSTRUCTIONS BEFORE COMPLETING FORM

1. REPORT NUMBER: NRL Memorandum Report 3970
2. GOVT ACCESSION NO.
3. RECIPIENT'S CATALOG NUMBER

4. TITLE (and Subtitle): (6) FLAME – A SLOW-FLOW COMBUSTION MODEL
5. TYPE OF REPORT & PERIOD COVERED: Continuing
6. PERFORMING ORG. REPORT NUMBER

7. AUTHOR(s): (10) Walter W. Jones and Jay P. Boris
8. CONTRACT OR GRANT NUMBER(s): (12) 37 p.

9. PERFORMING ORGANIZATION NAME AND ADDRESS: Naval Research Laboratory, Washington, DC 20375 — 61153N
10. PROGRAM ELEMENT, PROJECT, TASK AREA & WORK UNIT NUMBERS: NRL Problem Nos. 62H02-51 and 62C01-15 (CONTINUED)

11. CONTROLLING OFFICE NAME AND ADDRESS: Office of Naval Research, 800 N. Quincy Street, Arlington, VA 22203 — (11) 16 JUL 79
12. REPORT DATE: July 16, 1979
13. NUMBER OF PAGES: 36

14. MONITORING AGENCY NAME & ADDRESS (if different from Controlling Office): (14) NRL-MR-3970
15. SECURITY CLASS. (of this report): Unclassified
15a. DECLASSIFICATION/DOWNGRADING SCHEDULE

16. DISTRIBUTION STATEMENT (of this Report)

Distribution unlimited; approved for public release.

17. DISTRIBUTION STATEMENT (of the abstract entered in Block 20, if different from Report)

(16) RR011-09, RR024-02

18. SUPPLEMENTARY NOTES

This work was sponsored by the Office of Naval Research under Project No. RR011-09-41 and the Naval Research Laboratory under Project No. RR024-02-41.

19. KEY WORDS (Continue on reverse side if necessary and identify by block number)

Flame spread
Combustion
Enclosed fires
Transient reactive flow
Ignition

(17) RR011-09-41, RR024-02-41

20. ABSTRACT (Continue on reverse side if necessary and identify by block number)

We have developed a two-dimensional, time-dependent reactive flow model for studying the various aspects of combustion, including ignition, flame spread and plume formation. The basic model is a self-consistent slow-flow hydrodynamic algorithm with chemical reactions. Also included are the basic transport processes of molecular diffusion and thermal conductivity. The model is implemented so that other physical mechanisms, such as different chemical reaction schemes, turbulence models, heterogeneous phenomena, etc., can be included on a modular basis.

DD FORM 1 JAN 73 1473 EDITION OF 1 NOV 65 IS OBSOLETE S/N 0102-014-6601

SECURITY CLASSIFICATION OF THIS PAGE (When Data Entered)

251 950

alt

10. PROGRAM ELEMENT, PROJECT, TASK AREA & WORK UNIT NUMBERS (CONTINUED)

ONR Proj. No. RR011-09-41 and NRL Proj. No. RR024-02-41

CONTENTS

FLAME – A SLOW-FLOW COMBUSTION MODEL

I. Introduction

This paper describes FLAME, a detailed, two-dimensional, time-dependent numerical model of slow flow combustion systems. The model has been built around the solution of self-consistent hydrodynamics equations in the "slow flow" approximation and includes the basic transport processes of molecular diffusion and thermal conductivity. Other physical mechanisms, such as detailed chemical reaction schemes, turbulence models and heterogeneous phenomena etc.; can be included on a modular basis. This facilitates modifying geometries and modelling various processes peculiar to specific systems. In addition, as new models for turbulence and chemical kinetics become available, they can be added in a relatively straightforward manner.

The basic geometry of the FLAME model is cylindrically symmetric $(r - z)$[1]. Other geometries are possible, but for many problems of interest, namely gas jets, diffusion flames, fire spread, and turbulent mixing studies, this would appear to be the best geometry. The numerical model is fully two-dimensional in order to treat quantitatively processes such as buoyancy, convection, shear flow and turbulence, which cannot be treated sensibly in a one-dimensional calculation. A fully three-dimensional calculation using the same techniques is possible but would be significantly more expensive. An important aspect of our approach has been to improve the resolution of sharp gradients via Flux-Corrected Transport. Nevertheless, the basic model is Eulerian and hence resolution of gradients is necessarily limited.

The set of equations modelled in FLAME is

Manuscript submitted May 23, 1979.

$$\frac{d\rho}{dt} = -\rho\nabla\cdot\mathbf{V} \equiv -\rho D \tag{1}$$

$$\frac{d\vec{\xi}}{dt} = \nabla\times\left(\frac{\nabla P}{\rho}\right) - \vec{\xi}D + \nabla\times\left[\frac{\nabla\cdot\nu\,\nabla\mathbf{V}}{\rho}\right] \tag{2}$$

$$\frac{dD}{dt} = -\nabla\cdot\left(\frac{\nabla P}{\rho}\right) + [\xi^2 + \mathbf{V}\cdot\nabla^2\mathbf{V} - 1/2\nabla^2\mathbf{V}^2] + \nabla\cdot\mathbf{g} + \nabla\cdot\left[\frac{\nabla\cdot\nu\,\nabla\mathbf{V}}{\rho}\right] \tag{3}$$

$$\frac{d\epsilon}{dt} + \epsilon D = -\nabla\cdot P\mathbf{V} + \nabla\cdot K\nabla T + \left.\frac{\partial\epsilon}{dt}\right|_{\text{chem}} + \sum_i h_i\rho_i\mathbf{V}'_i \tag{4}$$

where $\epsilon \equiv \frac{1}{2}\rho\mathbf{V}^2 + \frac{P}{\gamma-1} + \rho\phi$ = total energy

and

$$\frac{d\rho_i}{dt} = -\rho_i\nabla\cdot\mathbf{V} - \nabla\cdot\rho_i\mathbf{V}'_i + \left.\frac{\partial\rho_i}{\partial t}\right|_{\text{chem}}. \tag{5}$$

This is a very general formulation. The approximations and assumptions which we use in solving these equations will be discussed in Section III. The symbols are

- ρ = total mass density (gm/cm^3)
- n = total (particle) density (#/cm^3)
- ρ_i = mass density of the ith species (gm/cm^3)
- n_i = particle density of the ith species (#/cm^3)
- $\mathbf{V}$ = bulk fluid velocity (cm/sec)
- ξ = $\nabla\times\mathbf{V}$ - vorticity (sec^{-1})
- D = $\nabla\cdot\bar{\mathbf{V}}$ - divergence of the velocity (sec^{-1})
- g = gravity (-980 cm/sec^2) - negative gravity points downward
- γ = c_p/c_v - ratio of specific heats of the fluid
- K = thermal conductivity coefficient (erg/cm-sec-°K)
- h_i = enthalpy of the ith species of the fluid (ergs/molecule)
- $\mathbf{V}'_i$ = diffusion velocity of the ith species (cm/sec)
- ν = viscosity coefficient (gm/cm/sec)
- P = pressure (dynes/cm^2)

V = volume of the container (cm^3)

D_{ij} = binary diffusion coefficient for species "i" through species "j" (cm^2/sec)

S_i = diffusion source term for the ith species (cm^{-1})

As this is a two-dimensional calculation, both the (r) and (z) components of V and V′ are carried. In addition, we require two more equations to close this set. We have used

$$P = nkT \tag{6}$$

for the relation between pressure, density and temperature, and

$$S_i = \sum_j \frac{n_i n_j}{n^2 D_{ij}} (\overline{V}'_j - \overline{V}'_i) \tag{7}$$

to relate the diffusion velocities to the other physical parameters. The quantities S_i and D_{ij} are defined and discussed in detail in Appendix I. The quantities $\{S_i\}$ are forcing terms for molecular diffusion which include density, pressure, and temperature gradients as well as differential body forces on the various species.

This 2D model has a rather general initialization and diagnostics capability in order to consider a variety of problems. The numerical model is designed to operate efficiently on a vector computer, thus demonstrating the value of vector computation even in complex problems such as reactive flow.

This paper discusses some of the details of the model, that is the actual form of Eqs. (1-7) used, the simplifying assumptions made, and their justifications. In Section II areas of potential application and the corresponding numerical difficulties which they present are discussed. Section III describes the numerical model in greater detail. The grid system, spatial differentiation, timestepping, diffusive transport, and chemical kinetics algorithms are discussed. Section (IV) discusses calculations which have been performed to benchmark the model in several difficult but well understood situations. These tests include comparisons with a one-

dimensional, fully compressible Lagrangian code and, for simple cases, comparison with a one-point analytic calculation. Agreement is quite good, and we have been able to define the limits of accuracy of the approximations and numerical algorithms which are used.

II. Problems to be Solved

There are several types of cylindrically symmetric problems to which this model can be applied. One example is a laminar gas jet, such as a bunsen burner or a flat plate burner, where the fuel and oxidizer may mix either prior to or after entering the combustion chamber. In either case there is no reason to expect macroscopic asymmetry in the azimuthal direction. However, species densities and temperatures very dramatically both above the ignition point and radially outwards from the jet center, even in steady state. The two problems differ significantly in the initial conditions required and the way in which the geometric boundary conditions are applied. One is a diffusion flame and the other a premixed flame. In the case of the premixed system, the processes of interest will be the jet and flame speed and the detailed chemical kinetics. For the diffusion flame, however, the physics is made more complicated by the fact that a finite time is required for the oxidizer to mix with the fuel. Computational models which are to be applied to these typical practical situations invariably require a non-uniform grid to resolve the combustion regions finely while limiting the overall number of grid points at which computations must be made. The problem here is one of widely disparate physically important space scales.

Buoyancy is a major effect in most diffusion flames and even in premixed systems it can be responsible for much of the flame dynamics. The computational problem introduced here is one of widely disparate fluid dynamic timescales. The slow flow algorithm used for the temporal integration of the fluid dynamic equations is a way to filter sound waves out of the equations so that timesteps much longer than the Courant step $\delta t \sim \delta x / C_s$ can be taken without

numerical instability. The standard approach of formulating an implicit pressure equation requires at least formal substitution of one equation, in finite difference form, into another and usually some form of additional numerical smoothing. The resulting algorithms do not resolve steep gradients well during convection. Flux-Corrected Transport (FCT) is a far superior convection algorithm but is intrinsically nonlinear and hence does not lend itself to implicit formulations. Therefore the slow flow algorithm, which is asymptotic rather than implicit in concept, allows the unlimited use of FCT to convect steep species and temperature gradients. By filtering out the fast sound waves, the physically important buoyancy and molecular diffusion timescales can be integrated inexpensively using only a few timesteps rather than hundreds of thousands.

Another class of important problems concerns turbulent mixing with reactions. Large-scale, quasi-stationary eddy structures are observed in most shear flow situations and these structures clearly play a vital role in the turbulent mixing process. While the full details of fully developed turbulent flow is beyond numerical simulation, these eddy structures, which are often two-dimensional, can be simulated accurately. Therefore FLAME is designed to allow calculation of these structures with and without self-consistent energy release from the chemical kinetics. The importance of convective acceleration in this kind of problem necessitates carrying the slow flow expansion to first order in the perturbed pressures, but this is relatively easy to do. The goal is to have a fluid dynamics model which can resolve these structures realistically as a basis for testing macroscopic turbulence closure models.

Another area of applicaton for FLAME is the phenomenological modelling of fire spread in enclosed spaces. For this class of problem, the extreme care taken to provide an accurate fluid algorithm with good timestep properties is almost overkill. Nevertheless, since FLAME is designed for detailed modelling, the extra accuracy and reliability of the fluid dynamics should

pay dividends as a basis for phenomenological and empirical modelling as well. To this end, methods for representing inflow-outflow conditions and interior structures and obstacles are being studied. Before such a model becomes complete, however, extensive additional numerical work will have to be undertaken to build a multidimensional radiation transport model capable of dealing equally accurately with volumes which are optically thick as well as optically thin.

III. Numerical Model

There are three aspects to the integration of the equations which describe the system: 1) spatial integration and differentiation; 2) time-stepping and integration of the energy (pressure) equation using the assumption of asymptotic relaxation, i.e. "slow-flow"; 3) physical transport and chemical kinetics.

III.1. Grid System — Spatial Integration and Differentiation

The cylindrical finite difference grid used in the numerical model is shown in Fig. (1). Spatial integration and differentiation is performed on this staggered grid. The representation of the fluid dynamics is inherently Eulerian, although rezoning and variable grid spacing are allowed at each time step. This allows computation of quantities such as $\nabla \cdot \mathbf{V}$ to fall automatically on the grid points where they must be used. For example, for the continuity equation, $\frac{d\rho}{dt} = -\rho\nabla\cdot \mathbf{V}$, whereas ρ is defined on the grid, $\mathbf{V}$ must be defined at interstitial points in order for $\nabla\cdot\mathbf{V}$ to appear on the same grid as ρ. In solving for $\mathbf{V}$, the reverse calculation of the velocity from and $\vec{\psi}$ and Φ, the stream function and velocity potential, is similarly straightforward if $\vec{\psi}$ and Φ are defined at the proper places. When mass flux, that is momentum, is a necessary quantity such as in calculating the diffusion velocities, the only quantities which then need to be averaged are the mass densities at the half-cell positions. Thus this staggered grid structure insures that effectively second-order accuracy is maintained in spatial integration, at

least for a uniform or slowly varying grid spacing. The grid and numerical model in general can be applied to Cartesian and spherical as well as cylindrical coordinates. The model is set up to make the change relatively easy, but the geometrical constants used in spatial differentiation as well as the axis boundary condition ($NR = 1$) would have to be changed.

The quantities defined at grid points are D, $\vec{\xi}$ ρ, $\{\rho_i\}$, T, p and Φ. The stream function $\vec{\psi}$ and velocity $\mathbf{V}$ are carried at the interstitial points shown in Fig. (1). The grid is staggered in this manner to 1) facilitate calculation of $\mathbf{V}$ from Φ and $\vec{\psi}$ (and the reverse of course), 2) to make the model conservative without resorting to exotic boundary conditions and, 3) to simplify the implementation of boundary conditions. In order to insure conservation of mass, for example, in a closed system, the flux of mass across a boundary must be zero. Thus we choose $\frac{\partial \Phi}{\partial r} = 0$ and $\vec{\psi} = 0$ at the outside cylindrical wall, as is shown in Fig. (1).

The self-consistent nature of this grid can best be seen by use of an example. Consider the $\nabla \cdot \mathbf{V}$ term in Eq. (1) as a source term in the Poisson equation

$$\nabla^2 \Phi = \nabla \cdot \mathbf{V} \tag{8}$$

The term $\nabla \cdot \mathbf{V}$ becomes

$$\nabla \cdot \mathbf{V} = \frac{V_z(i',j'+1) - V_z(i',j')}{Z(j'+1) - Z(j')} + \frac{R(i'+1)\, V_R(i'+1,j') - R(i')\, V_R(i',j')}{[R^2(i'+1) - R^2(i')]/2} \tag{9a}$$

$$\left| \begin{array}{l} i' = 1 \text{ to } NR \\ j' = 1 \text{ to } NZ \end{array} \right.$$

The term $\nabla^2 \Phi$ becomes (for equal spacing in R and Z)

$$\nabla^2 \Phi = \frac{\Phi_{i,j+1} - 2\Phi_{i,j} + \Phi_{i,j-1}}{[(Z(j+1) - Z(j-1))/2]^2} + \frac{\Phi_{i+1,j}\, R(i'+1) - 2\Phi_{i,j} R(i) + \Phi_{i-1,j}\, R(i')}{[R^2(i'+1) - R^2(i')]/2} \tag{9b}$$

also at (i, j) on the main grid. Thus Eq. (8) has the left hand and right hand sides of the equation specified at the same physical place. A similar relationship exists for $\mathbf{V}$ and $\vec{\psi}$ (or $\nabla \times \mathbf{V}$

and $\nabla \times \nabla \times \vec{\psi}$) but with values for $\vec{\psi}$ on a different staggered grid than that used for Φ. Thus the four velocity variables Φ, $\vec{\psi}$, V_R and V_Z must be on different grids in order to be self-consistent and conservative without resorting to artificial boundary conditions and/or excess averaging.

Equations (2) and (3), the curl and divergence of velocity respectively, require the calculation of velocity itself as a source term. In addition, velocity is a useful diagnostic tool and is used for other calculations as well. For simple theories, or low order approximations, the vorticity and divergence alone could be used. Such is not the case for our model and hence we need to be able to calculate the velocity from $\nabla \times \mathbf{V}$ and $\nabla \cdot \mathbf{V}$. This is easily done by defining a stream function $\vec{\psi}$ and velocity potential Φ by

$$\mathbf{V} = \nabla\Phi + \nabla\times\vec{\psi}.$$

This then leads to two equations for Φ and $\vec{\psi}$.

$$\nabla^2\Phi = \nabla \cdot \mathbf{V} = D \tag{10a}$$

and

$$\nabla\times\nabla\times\vec{\psi} = \nabla\times\mathbf{V} \equiv \vec{\xi}. \tag{10b}$$

These are elliptic equations of the general form

$$\left[A \frac{\partial^2}{\partial x^2} + B \frac{\partial^2}{\partial y^2} + C \frac{\partial^2}{\partial x \partial y} + D \frac{\partial}{\partial x} + E \frac{\partial}{\partial y} + G\right] \psi = F \tag{11}$$

with either Neumann or Dirichlet boundary conditions, both of which arise. Part of our original choice for the staggered grid was based on being able to set these boundary conditions easily. Thus Eq. (10) can be cast in the form

$$\nabla^2 \Phi = F_1 \tag{12a}$$

and

$$\nabla \times \nabla \times \vec{\psi} = \vec{F}_2 \tag{12b}$$

which are elliptic equations of the general form of Eq. (11). The substitution method of Madala[2] solves these equations more quickly than the usual relaxation methods and with more

accuracy than iterative schemes. Most important, however, is that it allows the coefficients A, B, C, D, E and F to be functions of both position and time which allows for stretched grids and simple rezoning.

III.2. Time Stepping and the Asymptotic Approximation

We have incorporated time-splitting in order to make the model flexible and to simplify adding modules to describe specific physical effects. Except for the driving program, which invokes the hydrodynamics, molecular diffusion and thermal conductivity, the various modules which incorporate the physical processes are exercised separately and interact as source terms at each time step. This splitting is a standard technique but the inherent assumptions must always be tested when implementing a new numerical model.

In FLAME all time-stepping is done explicitly in a time-centered fashion. Doing the calculation explicitly allows more flexibility in the model development. Time-centering ensures reversibility in the physics. By reversing the sign of the time step, δt, we can make the reversible physics run backwards. This is a real property in non-dissipative physical systems which ought to be mirrored as closely as possible in a numerical model. When diffusion is included, such reversibility ceases to be strictly valid of course.

Although explicit methods have time step limitations to avoid instability, our asymptotic pressure relaxation[1] algorithm is an exception to this general rule. To illustrate this point, we note that Equations (1), (2), and (5) are solved as is. However, Equations (3) and (4) are combined to form the following equation

$$\gamma PD = -\mathbf{V}\cdot\nabla P + \left[\left.\frac{\partial P}{\partial t}\right|_{\text{chem}} - \left\langle\frac{\partial P}{\partial t}\right\rangle_{av}\right] \tag{13}$$

$$+ (\gamma-1)\left[\nabla\cdot K\nabla T - \mathbf{V}\cdot(\nabla\cdot\nu\nabla\mathbf{V}) + \sum_i h_i\rho_i\mathbf{V}'_i\right]$$

where

$$<\frac{\partial P}{\partial t}>_{av} \equiv \frac{1}{V} \int dV(\{\gamma - 1\} \left.\frac{\partial \epsilon}{\partial t}\right|_{\text{chem}} \tag{14}$$

and finally

$$P_{\text{new}} = P_{\text{old}} + \delta t <\frac{\partial P}{\partial t}>_{av}. \tag{15}$$

Such a formulation embodies the assumption that waves travelling at the sound speed do not influence the overall hydrodynamics motion. This is the reason for the name "Slow-Flow".

This formulation excludes shock waves from the set of problems which we can consider. The pressure can still vary overall, but now only on the timescale of the chemical energy release. This is the time-stepping approach used in the solution of the energy equation. For Eqn. (1), (2) and (5) which are solved explicitly, we use flux-corrected transport[3-5]. The FCT method is both relatively non-diffusive, and very fast. The worst problem which arises using this method is the non-linear clipping phenomenon, which will be discussed in detail in the next section under results. Generally clipping occurs when there is a sharp peak in the mass density (ρ) or vorticity (ξ). The anti-diffusive flux terms (which allow very steep gradients to propagate conservatively) tend to flatten such peaks. As will be seen, this introduces little error even in the worst case, e.g., a Heaviside function of density or vorticity perturbation, and the error is virtually non-existent when small gradients are present.

The numerical timestep to which we are limited is the shortest of those required to integrate (stably) molecular diffusion, thermal conductivity and fluid flow. Chemistry computation is allowed to subcycle itself, so this will not limit the overall timestep unless so much energy is released that it affects the fluid flow and diffusion timestep limits. Typical time constants for molecular diffusion can be found from the diffusion equation cast into the form

$$\frac{1}{\rho} \frac{\partial \rho}{\partial t} \sim \frac{1}{\rho} \nabla \cdot (D \nabla \rho), \tag{16}$$

with

$$D \simeq \frac{10^{17} T^{3/4}}{n}. \tag{17}$$

Thus, for example, for temperatures in the range of 500-1000°K and a grid spacing of 0.25 cm, the diffusion limit timesteps will be about 0.1-0.01 seconds. These limits vary with time and must, of course, be checked at each timestep.

The equations are integrated using a time centered scheme. The order of the integrations is as follows:

1) Estimate values for P, ρ, $\{\rho_i\}$, $\vec{\zeta}$, D, T, $\vec{\psi}$, at Φ at the new time.

2) Find source terms for Eqn. (1, 2, 5 and 10) based on time centered values $(t_o + 1/2\ \Delta t)$.

3) Integrate Eq. (1, 2, 5 and 10) from (t_o) to $(t_o + \Delta t)$ using the source terms defined at the time centered position. This is a fluid flow calculation only.

4) Repeat steps (2) and (3) until convergence is reached.

5) Integrate the kinetics portion of Eqn. (5, 6, 13, 14 and 15) using the Asymptotic Chemical Kinetics Scheme of Young and Boris.[6] The subcycling done at this point effectively integrates the equation of state, and the energy release is accumulated as a source term for step (1).

The following illustration shows where each of these time-step points is, in relation to steps (1-5)

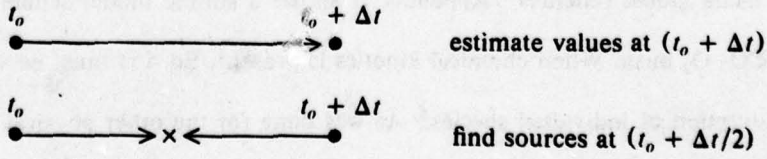

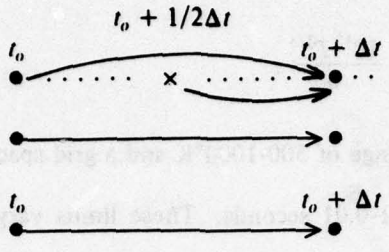

Since each step of the integration is of *at least* second order accuracy, the overall scheme will also be second under accurate. In addition, using the time centered source terms in steps (2 and 3) insures reversibility, at least for non-diffusive physical systems, once the iterative scheme has converged.

III.3. Physical Transport and Chemical Kinetics

There are two pieces of physics built into the model which are crucial to model any combustion problem accurately. Molecular diffusion and thermal conductivity have been built into the basic model. Both are essentially source terms in Eq. (13). At present, we use the conceptually simple results of Sears[7] for K_T, namely

$$K_T \sim 884\sqrt{\frac{32}{A}}\sqrt{\frac{T}{T_o}}, \tag{18}$$

where A is the average molecular mass of the gas and $T_o = 293°K$. For molecular diffusion, we calculate the actual diffusion velocities for each species from the fully coupled diffusion equations. *The method is discussed in detail in Appendix I.*

The chemistry portion of our model is a general five-species model. Such a configuration was chosen so that we could model such systems as CO-O_2 and O_3–O_2 in detail, or H_2–O_2 and and CH_4–O_2 using global schemes. Appendix II shows a simple model scheme and also the one used for CO–O_2 burn. When chemical kinetics is present, Eq. (5) must be solved for creation and consumption of individual species. As was done for the other physical effects, energy release or absorption is a source term in the energy equation, Eq. (13).

As in our choice of grid and hydrodynamic algorithms, we must strike a balance between physical complexity and model flexibility. More species can be added, of course, but having five species allows a large number of important calculations to be performed without detracting from the main purpose of FLAME which is to perform accurate multidimensional calculations. With five species we can model the CO-O_2 and the O_3–O_2 systems in detail. The H_2–O_2 system and more complex hydrocarbon systems such as methane and benzene can be modelled using global schemes. For the simple, detailed models we can even add diluents to test for flammability and flame extinction. For the global models of reactive systems the emphasis shifts to studying detailed fluid dynamic effects. The flow of trace species in nitrogen pressurization experiments can be followed and more realistic reaction schemes than $A + B \rightarrow C$ can be used for turbulent mixing calculations and calibration of turbulence closure models.

IV. Tests of the Model

In order to be able to trust the predictive capability of the model, as a minimum we must insure that it behaves properly in cases where we know the answer. The two aspects to checking this predictive capability involve benchmarking it against well documented and thoroughly tested numerical models and also against experiments for which we can reasonably expect good agreement and which have been well diagnosed.

We report here on the former set of tests, namely comparison with other models and calculations. In each case, where possible, we have compared this model with a one-dimensional fully implicit Lagrangian code and also a simple "analytic" model. The tests we applied were both passive, that is no reactions occurred, and active and hence included reactions. The former tests check the internal consistency of the hydrodynamics whereas the latter check the validity of the coupling of chemistry to the hydrodynamics. In both sets of tests, we used the Heaviside temperature perturbation[8] shown in Fig. (2) and given by

$$\rho = \begin{cases} \rho_o - \Delta\rho, & r \leqslant R_o \\ \rho_o, & r > R_o \end{cases} \quad R_o = 2.67\text{cm}.$$

The first set of tests were passive, that is no reactions were present. This would be the situation if only one species were present, or if the two initial species were oxygen and nitrogen. All combinations of molecular diffusion and conductivity were tried. Figure (3) shows the comparison between FLAME (●) and the Lagrangian one dimensional model (○) after three seconds with both mass diffusion and thermal conductivity included. By plotting the temperature as a function of radius in these figures the 2D data are collapsed into a simple 1D plot. The spread or scatter of the various FLAME temperature values near a given radius gives a good measure of the numerical truncation error because this scatter arises from performing a spherical calculation on a cylindrical r-z mesh. As can be seen, the agreement between the two is quite good even for relatively long times. Also, there is very little asymmetry in the 2D calculation. Near the peak, however, there is some clipping due to the use of the FCT routines on the rather coarse grid used for these tests (20×20). To assure ourselves that indeed the two codes would agree qualitatively we did one test on a (40×40) grid, shown in Fig. (4). Since we see errors of less than 5% in both cases the general problem of convective transport will be well handled, even on the rather coarse grid. When we turn to the problem of turbulence, however, we will need the resolution at particular grid points and then we can either use fine gridding, or variable grid spacing to obtain high resolution at the necessary points. The latter technique, called variable rezoning, is presently being worked on.

One necessary test was a check of molecular diffusion when only one species was present, that is

$$\rho = \rho_A,$$

or when equal parts of two species are present, which have the same mass, and are in all other aspects identical. In such a situation, there should be no net diffusion. This is the same as say-

ing that there is no diffusion of the total mass density due to molecular diffusion. This was verified for both the one and two-dimensional models and is attributable to the manner in which we calculate the diffusion velocities.

These tests have validated the internal consistency of the hydrodynamic parts of the model. Next we tested the basic assumption of time-step splitting. The first check was of the chemistry in a configuration where hydrodynamics could not play a part. Such is the case when uniform ignition is used, namely,

$$\rho = \rho_A + \rho_B, \; \rho_A = \rho_B$$

and

$$\rho = \rho_o - \Delta\rho$$

for all radii. For these conditions there will be no transport. All three models (including the one point analytic model) agreed to within one degree Celsius, which is adequate. For asymptotic calculations of the sort in which we are interested, which last for tens of seconds, shortening the timestep to the chemistry time scale (as was necessary in the previous calculation) is not a satisfactory solution. Instead, we chose to subcycle the chemical kinetics and couple this to the hydrodynamics by accumulating the source terms for all subcycles and updating the equation of state at each subcycle. An independent equation for the temperature based on energy release could have been solved, but we have found stability problems in this approach. The technique of subcycling allows us to use a hydrodynamics timestep of one to two orders of magnitude larger than that required for the chemical kinetics.

The validity of this approach is demonstrated by the calculation which is shown in Fig. (5). In (5a) the bubble radius is plotted and in (5b) the peak temperature is shown, both as a function of time. In both cases, the points (O) represent the (2D) calculations, and the points (•) represent the equivalent (1D) calculation. As can be seen, the peak temperatures, ignition

times, and bubble radius agree satisfactorily. For these computations, only chemistry and the fluid flow are allowed to play a part. Both molecular diffusion and thermal conductivity are absent.

To complete this series of tests, which checks the symmetry of the two-dimensional model as well as comparing it with a well documented one-dimensional model and a single "analytic" one point model, we ran a test with molecular diffusion, thermal conductivity, chemistry and hydrodynamics, all interacting. Figure (6) shows a plot of the temperature profile for FLAME (●) and the Lagrangian one-dimensional model (○), in this configuration. As can be seen, differences between the three models are quite small. Temperature has been used as a diagnostic for two reasons: first, it is sensitive to errors in both the hydrodynamics and chemical kinetics; second, it is a straightforward physical quantity and is easily visualized and measured. Asymmetries which appear can then be discussed in terms of too great (or too small) a flow or too much energy release. If the two dimensional hydrodynamics were done incorrectly, it would most likely show up as an asymmetry, and if either the hydrodynamics or the chemistry were incorrect, a difference between the temperature profiles of the two models would be apparent.

V. Conclusions

As can be seen, the FLAME implementation of the reactive flow model in two dimensions agrees well with both one point analytic calculatons as well as with a well tested one dimensional model. Furthermore, it is conservative both for mass and energy. The early problems to be modeled should be those for which well diagnosed experiments exist. Eventually, however, one will want to attempt predictions for systems which are in the design phase or for which experimental data are difficult or impossible to obtain.

The potential applications of this model are numerous and expand still further when certain modifications and extensions of the model are contemplated. Using the code in its current form, a number of gas jet and burner problems are being considered which will contribute to the interpretation of chemical kinetics investigations ongoing in a number of laboratories. In these cases rather detailed kinetics packages will have to be incorporated but laminar diffusion and premixed flames will be used so that turbulence will not cloud the reaction kinetics issues. The basic FLAME code will be equally useful in treating heterogeneous combustion and turbulent mixing because the basic hydrodynamics is about as accurate and non-diffusive as is possible in an Eulerian representation. By simplifying the chemistry and concentrating on the flow complications, extensive turbulent fields can be simulated with and without subgrid turbulence closure models. In special cases FLAME can be used to evaluate, via simulation, the probability density functions which are often invoked in turbulence modelling, but are not known accurately.

VI. Acknowledgments

This work was sponsored by the Office of Naval Research under Task # RR011-09-41 and through the block funding program Task # RR024-02-41. Also many thanks are due to the many people who have taken the time to proof read the manuscript and check the validity of the equations and approximations used.

REFERENCES

1. W. W. Jones and J. P. Boris, J. Phys. Chem. **81**, 2532 (1977).

2. R. V. Madala, Month. Weat. Rev. **106**, 1735 (1978).

3. J. P. Boris and D. L. Book, J. Comp. Phys. **11**, 38 (1973).

4. D. L. Book, J. P. Boris and K. Hain, J. Comp. Phys. **18**, 248 (1975).

5. J. P. Boris and D. L. Book, J. Comp. Phys. **20**, 397 (1976).

6. T. R. Young and J. P. Boris, J. Phys. Chem **82**, 2424 (1977).

7. F. W. Sears, "An Introduction to Thermodynamics, The Kinetic Theory of Gases and Statistical Mechanics," Addison-Wesley, Reading, Mass. (1964).

8. R. W. Bracewell, "The Fourier Transfer and Its Application", McGraw Hill, New York, (1965).

9. F. Williams, "Combustion Theory", Addison-Wesley, Reading, Mass. (1964).

Appendix I

Multi-species diffusion velocities can be related to those due to binary diffusion by considering the general diffusion equation[9]

$$\nabla(n_i/n) = \sum_{j=1}^{N} \left[\frac{\mu_{ij}\nu_{ij}}{P}\right](\mathbf{V}'_j - \mathbf{V}'_i) + \left[\frac{\rho_i}{\rho} - \frac{n_i}{n}\right]\frac{\nabla P}{P} + \frac{\rho}{P}\sum_{j=1}^{N}\frac{n_i n_j}{n^2}(\mathbf{f}_i - \mathbf{f}_j) + \sum_{j=1}^{N}\left[\frac{\mu_{ij}\nu_{ij}}{P}\right]\left[\frac{D_{T_j}}{\rho_j} - \frac{D_{T_i}}{\rho_i}\right]\frac{\nabla T}{T} \tag{I.1}$$

where N is the number of species, μ_{ij} is the reduced mass, fi represents the body force on the i th species and ν_{ij} is the binary viscosity coefficient. If we use the usual definition for the binary diffusion coefficient, namely

$$D_{ij} = \frac{n_i n_j P}{n\nu_{ij}\mu_{ij}}, \tag{I.2}$$

then Eq. (I.1) becomes

$$\nabla(n_i/n) = \sum_{j=1}^{N}\left[\frac{n_i n_j}{n^2 D_{ij}}\right](\mathbf{V}'_j - \mathbf{V}'_i) + \left[\frac{\rho_i}{\rho} - \frac{n_i}{n}\right]\frac{\nabla P}{P} + \frac{\rho}{P}\sum_{j=1}^{N}\frac{n_i n_j}{n^2}(\mathbf{f}_i - \mathbf{f}_j) + \sum_{j=1}^{N}\frac{n_i n_j}{n^2 D_{ij}}\left[\frac{D_{T_j}}{\rho_j} - \frac{D_{T_i}}{\rho_i}\right]\frac{\nabla T}{T}. \tag{I.3}$$

We can cast this into an implicit form by defining as a source term, all those elements of Eq. (I.3) which are not explicitly velocity dependent, namely

$$\mathbf{S}_i \equiv \nabla(n_i/n) - \left[\frac{\rho_i}{\rho} - \frac{n_i}{n}\right]\frac{\nabla P}{P} - \sum_{j=1}^{N}\left[\frac{n_i n_j}{n^2 D_{ij}}\right]\left[\frac{D_T}{\rho_j} - \frac{D_T}{\rho_i}\right]\frac{\nabla T}{T} - \frac{\rho}{P}\sum_{j=1}^{N}\frac{n_i n_j}{n^2}(\mathbf{f}_i - \mathbf{f}_j) \tag{I.4}$$

The third source term in Eq. (I.4) is diffusion due to thermal gradients. It is included because there are situations in which it can be important, especially when there are heavy and light species mixing, e.g., hydrogen and oxygen. With this definition for source terms, Eq. (I.3) can be written in the form

$$\mathbf{S}_i = \sum_{j=1}^{N} \frac{n_i n_j}{n^2 D_{ij}} (\mathbf{V}'_j - \mathbf{V}'_i). \tag{I.5}$$

Since $\sum_i S_i = 0$ and on the right hand side of Eq. (I.5) there are only $N-1$ independent terms, Eq. (I.5) is singular. Therefore, we require one more equation to close this set. For this, we use the physical condition

$$\sum_i \rho_i \mathbf{V}'_i \equiv 0, \tag{I.6}$$

which implies that the total mass continuity equation has no net diffusion term.

In order to make this a more tractable problem, we assume that the diffusion velocities separate into directions associated with the vector gradients. Then the equations to be solved become two dimensional matrix equations (in species), rather than a full-blown tensor equation. Thus we have

$$S_i = \sum_{j \neq i}^{N} \frac{n_i n_j}{n^2 D_{ij}} (V'_j - V'_i), \tag{I.7}$$

with the mutual term dropped explicitly. This term allows us to define a diffusion coefficient for each species relative to the rest of the fluid, in the spirit of the binary diffusion coefficient. Define

$$D_{i\Sigma} \equiv \frac{n - n_i}{\sum_{k \neq i}^{N} n_k / D_{ik}} \tag{I.8}$$

as an average diffusion coefficient. It has the following properties:

1. In the case of two species, it reduces to the binary diffusion coefficient.
2. It has the same symmetry properties as the reduced mass (μ_{ij}).
3. It will be the same for two species which behave identically.
4. Reduces to zero for a single species.
5. Allows us to make a perturbation expansion for the diffusion velocities in terms of the diffusion coefficient and the source term, S_i.

Defining a perturbation series for V', we have

$$V'_i = V_i^o + \delta V_i + \delta(\delta V_i) + \ldots\ldots \tag{I.9}$$

and substituting into Eq. (I.8) yields

$$S_i = \sum_{j\neq}^{N} \frac{n_i n_j}{n^2 D_{ij}}([V_j^o - V_i^o] + [\delta V_j - \delta V_i] + [\delta\delta V_j - \delta\delta V_i] + \ldots). \tag{I.10}$$

A judicious choice for V_i^o

$$V_i^o = -\left[\frac{\rho - \rho_i}{\rho}\right] \frac{n^2 D_{iN}}{(n - n_i) n_i} S_i \tag{I.11}$$

will allow us to make the corresponding expansion for

$$S_i = S_i^o + \delta S_i + \ldots.$$

By substitution we find

$$\delta V_i = -\left[\frac{\rho - \rho_i}{\rho}\right] \frac{n^2 D_{iN}}{(n - n_i) n_i} \delta S_i, \tag{I.12a}$$

$$\delta\delta V_i = -\left[\frac{\rho - \rho_i}{\rho}\right] \frac{n^2 D_{iN}}{(N - n_i) n_i} \delta\delta S_i \tag{I.12b}$$

etc. where

$$\delta S_i = \sum_{k\neq i}^{N} \left[\frac{\rho_i}{\rho}\delta_{ik} + \frac{n_i}{D_{ik}}\left[\frac{\rho - \rho_k}{\rho}\right] \frac{D_{kN}}{(n - n_k)} (1 - \delta_{ik})\right] S_k = \sum_k A_{ik} S_k \tag{I.13a}$$

$$\delta\delta S_i = \sum_{k,l} A_{ik} A_{kl} S_l \qquad \text{etc.} \tag{I.13b}$$

Combining terms yields, given the above definition for A,

$$V'_i = -\left(\frac{\rho - \rho_i}{\rho}\right) \frac{n^2 D_{iN}}{(n - n_i) n_i} (\bar{\bar{1}} + \bar{\bar{A}} + \bar{\bar{A}}\,\bar{\bar{A}} + \bar{\bar{A}}\,\bar{\bar{A}}\,\bar{\bar{A}} + \ldots.)\bar{S} \tag{I.14}$$

where the vector $\bar{S}$ is now over species. The problem we are left with is the convergence of this series. The convergence criterion is that

$$\left|\sum_{i,k} A_{ik}\, S_k\right| < \left|S_i\right| \tag{I.15}$$

which is necessary if Eq. (I.10) is to converge term by term. This can be shown to be true by substituting the above definition for A into the converge criterion (I.15). Then we have

$$\begin{aligned}
&\sum_{i=1}^{N} \sum_{k=1}^{N} A_{ik}\, S_k = \sum_{k=1}^{N} S_k \sum_{i=1} A_{ik} \\
&- \sum_{k=1}^{N} S_k \sum_{i=1}^{N} \left[\frac{\rho_i}{\rho}\,\delta_{ik} + \frac{n_i}{D_{ik}} \left[\frac{\rho - \rho_k}{\rho}\right] \frac{D_{kN}}{(n - n_k)} (1 - \delta_{ik})\right] \\
&- \sum_{k=1}^{N} \frac{\rho_k}{\rho}\, S_k + \sum_{k=1}^{N} \left[\frac{\rho - \rho_k}{\rho}\right] \frac{D_{kN}}{(n - n_k)} \sum_{i \neq k}^{N} \frac{n_i}{D_{ik}} \\
&- \sum_{k=1}^{N} S_k \equiv 0.
\end{aligned} \tag{I.16}$$

Thus the series (I.10) should converge. The above only insures conditional convergence rather than absolute convergences. However, we have found that in all practical calculations the series (I.10) converges to within 1% after two iterations.

Numerically, however, there may be a problem with differences of large numbers producing round-off errors. Addition of a constant $\{C\}$ to each row of matrix A does not change the value of δV_i, since by application of Eq. (I.16), the transformation

$$A'_{ik} = A_{ik} - C_i \tag{I.17}$$

leaves δV_i, $\delta\delta V_i$ etc., unchanged. Since the choice of $\{C\}$ is arbitrary, we chose it so that the mean value of each row of A vanishes,

$$C_i = \frac{1}{N} \sum_{i=1}^{N} A_{ij} \tag{I.18}$$

and thus the "difference-in-large-numbers" problem is solved prior to finding the δV's etc.

We have implemented the above diffusion model in a subrountine called DFLUX, which has been optimized for a vector computer. In the two dimensional model, we find the diffusion fluxes for all species for each layer in the radial direction. Thus the natural vector length will be $NR \times NSP$ in length where NR represents the number of grid points in a horizonal layer and NSP is the number of species. Figure (7) shows the time required to calculate the $\{n_i V_i\}$ for each of these layers for a 10×10, 20×20, 40×40 and finally an 80×80 grid, with five species at each grid point. As can be seen, the computation time required for each grid increases much more slowly than the number of grid points. A more dramatic demonstration of this is shown in Figure (8) where the time required for each grid point is plotted as a function of the layer size, with the total grid being held constant at 400 points. The times are normalized to the time required for a single point (+) and for a vector of length ten (•). The two curves approach, asymptotically, the speed limitation of the computer hardware.

For more than about ten grid points this method is faster than calculation of the usual diffusion source term $\nabla \cdot (D \nabla \rho)$ usually used as a source term in the momentum equation, and in addition is a more satisfactory approach.

Appendix II

Both the model chemistry and the carbon monoxide schemes are five species models. We have used the model chemistry for testing, however, since we know its time history on a theoretical basis.

For the model chemistry, species four and five are used simply as diluent. This allows a more satisfactory treatment of the scheme A + B → C due to momentum and energy conservation considerations, but is solved just as quickly. All rates are in a simplified Arrhenius form

$$R_i = C_i \exp(-E_i/T).$$

The values for the coefficient C_i and E_i are given in Table (I).

Table I

Species	C	E
1	4.8×10^{-14}	6.0×10^{3}
2	5.0×10^{-33}	6.0×10^{3}
3	$9.6 \times 10^{+4}$	7.0×10^{3}
4	1.0×10^{-14}	7.0×10^{3}
5	0.0	7.0×10^{3}

The scheme is

$$\frac{dn_5}{dt} = \frac{dn_6}{dr} = 0 \tag{II.1}$$

$$\frac{dn_1}{dt} = \frac{dn_2}{dt} = -\frac{dn_3}{dt} \tag{II.2}$$

and

$$\frac{dn_1}{dt} = R_3 n_3 + R_4 n_3 \cdot n - R_1 \cdot n_1 \cdot n_2 - R_2 \cdot n_2 \cdot n. \tag{II.3}$$

This scheme thus allows for both two and three body interactions.

This carbon monoxide scheme is somewhat more complex. We solve the following set of equations which also correspond to the source terms in Eq. (5).

$$\frac{d}{dt}[CO] = -C_{2f}[CO][O][M] - C_{3f}[CO][O_2] \tag{II.4}$$
$$+ C_{2R}[CO_2][M] + C_{3R}[CO_2][O]$$

$$\frac{d}{dt}[O_2] = + C_{1f}[O]^2[M] - C_{3f}[CO][O_2] \tag{II.5}$$
$$- C_{1R}[O_2][M] + C_{3R}[CO_2][O]$$

$$\frac{d}{dt}[O] = - 2C_{1f}[O]^2[M] - C_{2f}[CO][O][M] + C_{3f}[CO][O_2] \tag{II.6}$$
$$+ 2C_{1R}[O_2][M] + C_{2R}[CO_2][M] - C_{3R}[CO_2][O]$$

$$\frac{d}{dt}[CO_2] = + C_{2f}[CO][O][M] + C_{3f}[CO][O_2] \tag{II.7}$$
$$- C_{2R}[CO_2][M] - C_{3R}[CO_2][O].$$

We then have the following correspondence with the $\{n_i\}$,

$n_1 = [CO]$
$n_2 = [O_2]$
$n_3 = [O]$
$n_4 = [CO_2]$

and n_5 = a diluent whose total density is fixed, that is $\frac{dn_5}{dt} \equiv 0$. These equations correspond to the following reactions

	Forward (f)	Reverse (r)
(1)	$O + O + M \rightarrow O_2 + M$	$O_2 + M \rightarrow O + O + M$
(2)	$CO + O + M \rightarrow CO_2 + M$	$CO_2 + M \rightarrow CO + O + M$
(3)	$CO + O_2 \rightarrow CO_2 + O$	$CO_2 + O \rightarrow CO + O_2$.

The general form of the rate coefficients is

$$C = C_\phi T^\alpha e^{-E/T}$$

and the coefficients are given in Table (II).

Table II

Reaction	C_ϕ (f)	α (f)	E(f)	$C_\phi(r)$	α(r)	E(r)
1	5.2×10^{-35}	0	−900	3.0×10^{-6}	−1	59350
2	1.4×10^{-32}	0	900	2.6×10^{-3}	−0.87	64910
3	4.2×10^{-12}	0	24000	2.8×10^{-11}	0	26500

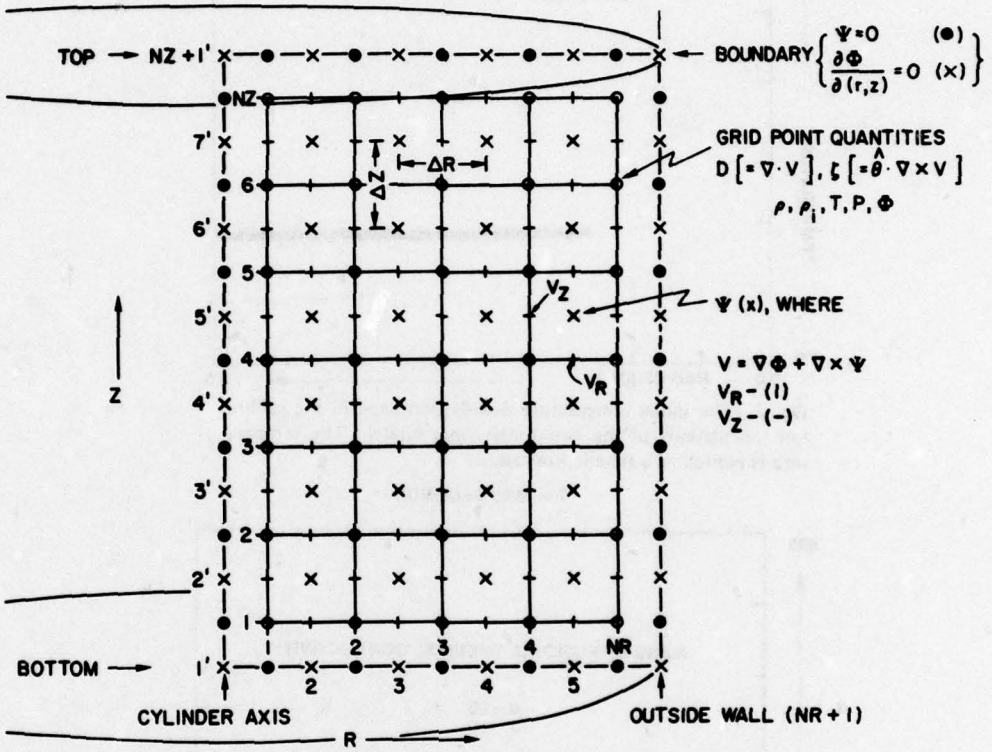

Fig. 1. Schematic diagram of the grid system used in the two-dimensional flame model. The figure shows a staggered grid and indicates where each variable is defined.

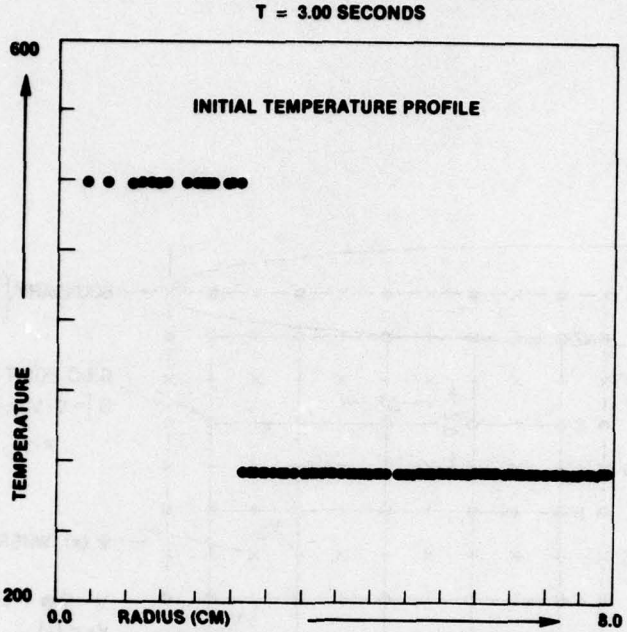

Fig. 2. The initial temperature distribution used in the calibration calculations of the two-dimensional model. The temperature is plotted as a function of radius.

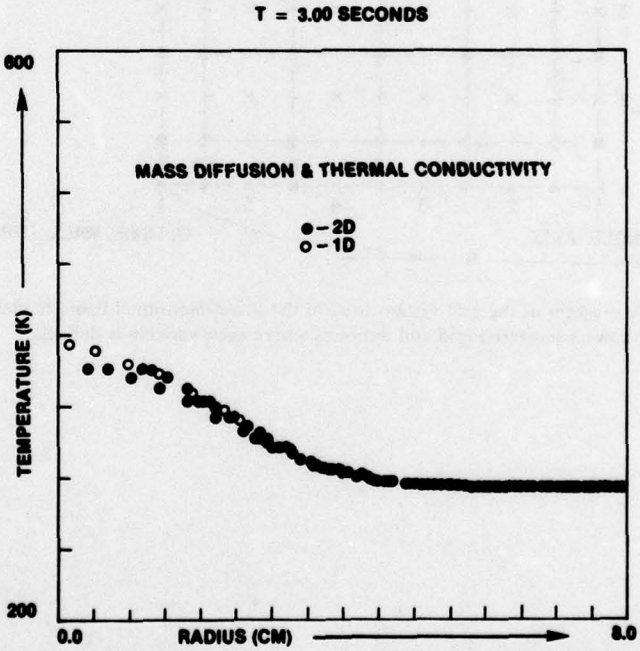

Fig. 3. Scatter plot of temperature verus radius when both molecular diffusion and thermal conductivity are included. The scatter arises from doing a spherically symmetric calculation on a cylindrical grid. The initial condition for this calculation is shown in Fig. (2). A scatter plot of this type reveals any grid induced asymmetries in the 2D numerical model. In addition, this representation is a convenient vehicle for comparison with the 1D model.

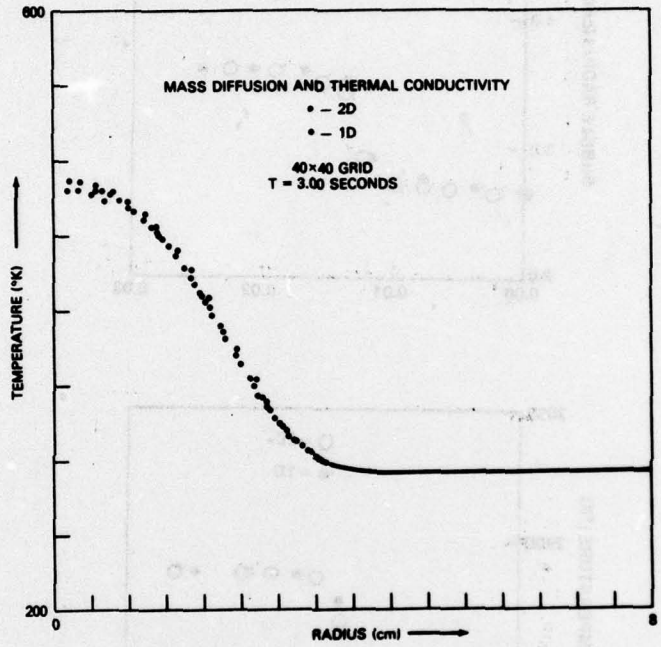

Fig. 4. Scatter plot of temperature versus radius for the same problem as shown in Fig. (2) and (3). This calculation is performed with a grid spacing, in both r and Z, which is one half the previous value (twice as well resolved).

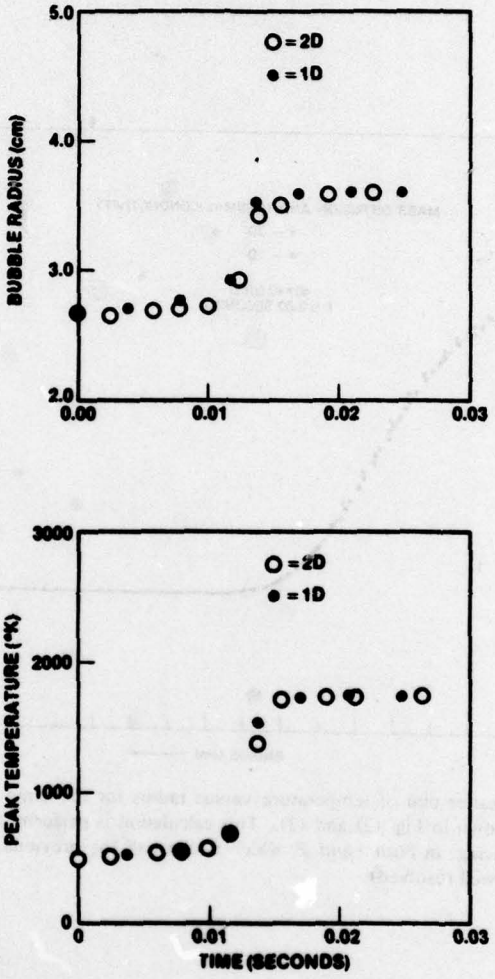

Fig. 5. Plot of peak temperature and bubble radius when chemistry is included and there is no mass diffusion nor thermal conductivity. The initial temperature profile is shown in Fig. (2). Since diffusion and conductivity are absent, the initial bubble will expand as the interior burns but will finally reach an equilibrium value with the region exterior to the bubble unburned. Heating of the exterior region is due only to compression.

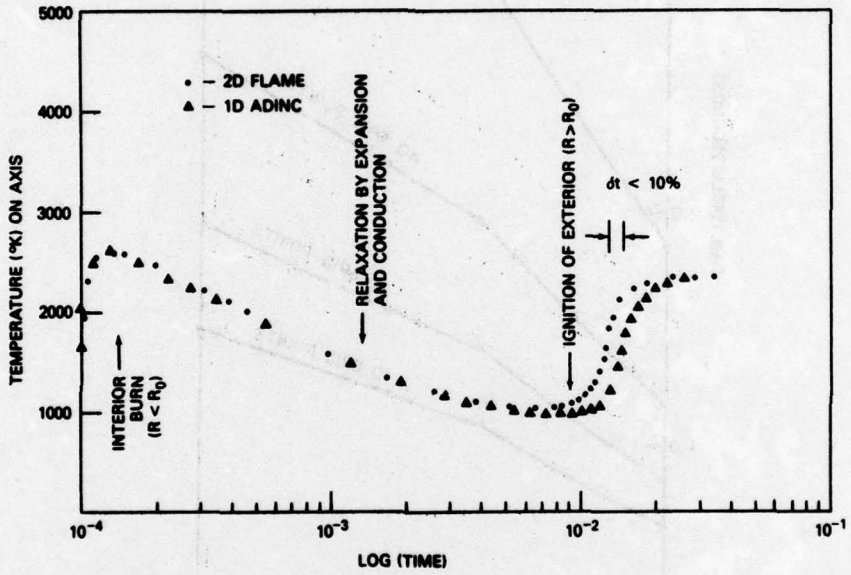

Fig. 6. Central temperature as a function of time. The initial conditions for this calculation are similar to those shown in Fig. (2) except $R_{max} = 0.2$ cm and $R_o = 0.067$ cm. In the previous calculation, Fig. (5), the exterior region did not burn. This calculation, however, includes reactions, conductivity and diffusion. Thus a flame front propagates from the interior to the outside wall. This front is coincident with the location of the maximum fluid divergence.

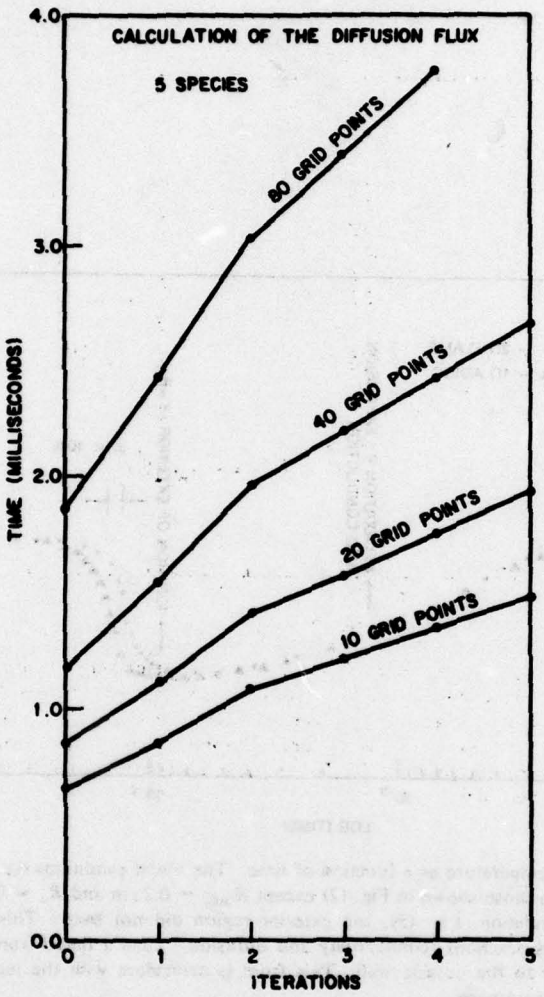

Fig. 7. Computation time required to calculate the diffusion velocities for all species at all grid points (with the number of grid points shown along each curve). As can be seen, the computation time increases more slowly than the number of grid points as vector overhead diminishes in importance.

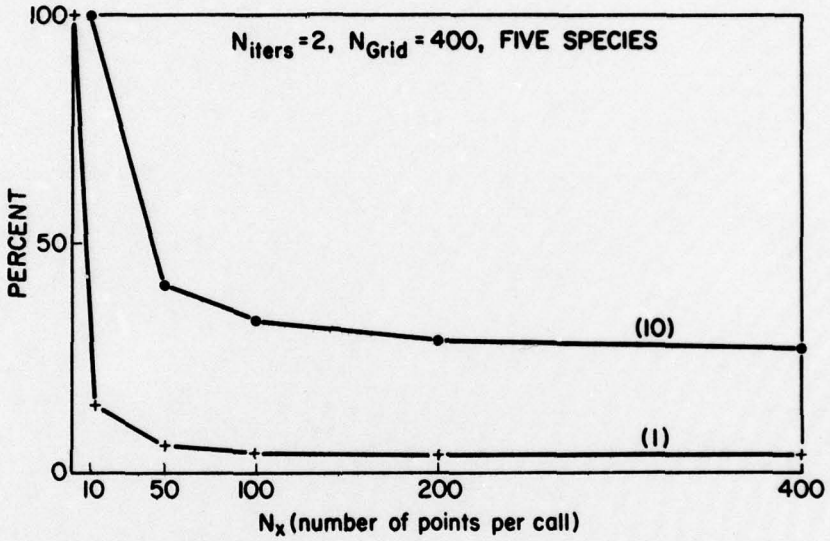

Fig. 8. A plot of the total time required to calculate the diffusion velocities for five species on a grid of four hundred points. The time is expressed as a percentage of the time required to do this calculation with a vector of length one (1) and a vector of length ten (10).